3D Inversion of Large-scale Time Domain Electromagnetic Data

Christoph Schwarzbach
University of British Columbia
Vancouver, British Columbia
cschwarz@eos.ubc.ca

Elliot Holtham
Computational Geosciences Inc.
Vancouver, British Columbia
elliot@compgeoinc.com

Eldad Haber
University of British Columbia
Vancouver, British Columbia
haber@math.ubc.ca

SUMMARY

Airborne time-domain electromagnetic (EM) surveys are effective tools for mineral exploration, geologic mapping and environmental applications. 3D inversion of airborne electromagnetic data is a challenging computational problem. The size of the surveys and the spatial resolution required to adequately discretize the transmitters and receivers results in very large meshes. Solving the forward problem repeatedly on such a mesh can quickly become impractical. Fortunately, using a single mesh for both the forward and inverse problem for all of the transmitters is not necessary. The forward problem for a single source or a small group of sources can be solved on different meshes, each of which need only be locally refined with fine cells close to the selected transmitters and receivers. Away from the selected transmitters and receivers, the mesh can be coarsened. The forward problem can then be broken into a number of highly parallel problems. Each forward modelling mesh is optimized specific to the selected transmitters and receivers and has far fewer cells than the fine inversion mesh. In this abstract, we present an implementation of this idea using a finite volume discretization on OcTree meshes. We demonstrate our approach on a VTEM data set over a porphyry deposit in Canada.

Key words: Electrical and EM methods, AEM, modelling, geophysical inversion

INTRODUCTION

Airborne time-domain electromagnetic (EM) surveys are effective tools for mineral exploration, geologic mapping and environmental applications. These surveys can be an economical way to explore large prospective regions. Traditionally, the data from such surveys have been interpreted using time constant analysis, conductivity to depth imaging (CDI) or possibly 1D inversion. These methods assist in a simple interpretation of the data; however, because they do not fully model the physics in 3D, they can fail to accurately represent environments such as real world structures and geological targets. Airborne EM datasets are characterized by large volumes of data, as each EM sounding implies a new transmitter location. As a result, inverting this data in 3D is a computationally difficult problem that until recently has not been possible for the exploration community.

The airborne electromagnetic (AEM) inverse problem (for example Haber et. al (2007) and Cox and Zhdanov (2008)) constitutes finding the spatial distribution of subsurface electrical resistivity which explains the observed data within the limits of the measurement uncertainties. To find such an earth model, one must solve the forward problem, the computation of the predicted data given a resistivity model. When solving the forward problem for AEM surveys, one faces a number of challenges. The first is the significant number of source locations. Controlled source airborne systems consist of a single moving transmitter and receiver that are flown across the survey area by an aircraft. Typical airborne systems record a new sounding every few meters. For airborne surveys where hundreds to tens of thousands of line kilometres of data are collected, a new sounding every few meters can result in thousands to millions of distinct source locations. Typically, the time to solve the forward problem scales linearly with the number of sources; therefore, it is critical that the forward problem is solved very efficiently. The second difficulty is a problem of scales. AEM surveys can cover large areas and aim at resolving both small- and large-scale variations of the subsurface resistivity. To this end, we introduce a mesh which subdivides the subsurface into cells and we seek to find the resistivity value in each of the cells. The mesh needs to cover the whole survey area to consistently account for large-scale features that may influence the data even at a considerable distance from the transmitter location. At the same time, the mesh cell size needs to be fine enough to recover the small-scale features and to reflect the spatial resolution of the data. This easily leads to meshes with millions of cells.

While a globally fine mesh is well designed for solving the inverse problem, it is not well suited to solve the forward problem since there are too many cells and each forward solve would be extremely time consuming and computationally demanding. To solve the forward problem for the ith transmitter–receiver pair, the local nature of the measurement only requires that the mesh cells are fine in the vicinity of the transmitter and the receiver. Far from the data the cells can be coarsened and be very large. Such a mesh has far fewer cells than the globally fine inverse problem mesh. Reducing the number of cells greatly accelerates the solution of the forward problem since the linear solvers involved scale superlinearly with the number of unknowns. Using smaller forward problem meshes allows direct solver methods to be used which are efficient when solving with many right hand sides and many time steps.

In this abstract, we present the implementation of an inversion algorithm which uses a globally fine mesh to solve the inverse problem and a number of locally fine meshes to solve the forward problem for selected transmitter–receiver pairs. The forward meshes can be chosen to accommodate a single source or a group of sources. Despite increasing the number of

cells, grouping sources might lead to an overall faster execution time because the total number of meshes, the total memory footprint, and some computational overhead is reduced. This work extends our previous work on time domain electromagnetics inversion using a single regular mesh (Haber et al., 2007) to OcTree meshes. The underlying regular structure of OcTree meshes greatly simplifies mesh handling and algorithmic development, compared to the finite element method on unstructured tetrahedral meshes (Günther, Rücker and Spitzer, 2006; Schwarzbach et al., 2011). A similar approach has been published by Cox and Zhdanov (2008). While Cox and Zhdanov (2008) first demonstrated the use of footprint based approaches to solve the forward problems arising from AEM data, we discretize the whole domain and refine the cells far from the transmitters to be coarse. Our approach offers the flexibility to adjust the cell size and can handle large conductors which can influence the measurement even from a great distance.

FORWARD PROBLEM

We formulate the forward problem as an initial boundary value problem in terms of the magnetic field $H_i(x,t)$,

$$\nabla \times \left(\rho(x) \nabla \times \mathbf{H}_i(x,t) \right) + \mu(x) \partial t \boldsymbol{H}_i(x,t) = \nabla \times \left(\rho(x) \nabla \times \boldsymbol{H}_{i0}(x) f(t) \right) \quad (1)$$

for $x \in \Omega$ and $t \in (0, T]$. The initial conditions are given as

$$\boldsymbol{H}_i(x,0) = \boldsymbol{H}_{i,0}(x) \quad , \quad (2)$$

and the boundary conditions are

$$\boldsymbol{n} \times (\rho(x) \nabla \times \boldsymbol{H}_i(x,t)) = \mathbf{0} \quad (3)$$

for $\in \partial\Omega$. Here ρ is the electrical resistivity and μ the magnetic permeability. The subscript i indicates the ith transmitter which we model by a current loop which carries a current f (t). For $t \leq 0$, we assume that f (t) = I_0 is constant, giving rise to the magnetostatic field $\mathbf{H}_{i,0}(x)$ which satisfies

$$\nabla \cdot \left(\mu(x) \boldsymbol{H}_{i,0}(x) \right) = 0 \quad (4)$$

We discretize the initial boundary value problem (1) in space using the finite volume method on OcTree meshes (Haber and Heldmann, 2007; Horesh and Haber, 2011) and in time using the backward Euler method. This yields a system of linear equations which can be written in compact form as

$$\boldsymbol{A}_i(\boldsymbol{m}) \boldsymbol{u}_i = \boldsymbol{b}_i(\boldsymbol{m}) \quad (5)$$

where

$$\mathbf{A}_i(\boldsymbol{m}) = \begin{pmatrix} \mathbf{M}_i + \delta t_1 \mathbf{K}_i(\boldsymbol{m}) & & & \\ -\mathbf{M}_i & \mathbf{M}_i + \delta t_2 \mathbf{K}_i(\boldsymbol{m}) & & \\ & \ddots & \ddots & \\ & & -\mathbf{M}_i & \mathbf{M}_i + \delta t_n \mathbf{K}_i(\boldsymbol{m}) \end{pmatrix} \quad (6)$$

$$\boldsymbol{u}_i = \begin{pmatrix} \boldsymbol{h}_{i,1} \\ \boldsymbol{h}_{i,2} \\ \vdots \\ \boldsymbol{h}_{i,n} \end{pmatrix} \text{ and}$$

$$\boldsymbol{b}_i(\boldsymbol{m}) = \begin{pmatrix} (\mathbf{M}_i + \delta t_1 f_1 \mathbf{K}_i(\boldsymbol{m})) \boldsymbol{h}_{i,0} \\ \delta t_2 f_2 \mathbf{K}_i(\boldsymbol{m}) \boldsymbol{h}_{i,0} \\ \vdots \\ \delta t_n f_n \mathbf{K}_i(\boldsymbol{m}) \boldsymbol{h}_{i,0} \end{pmatrix}. \quad (7)$$

Here, $\mathbf{M}_i$ is the mass matrix resulting from the finite volume discretization of the time derivative term in equation 1, and $\mathbf{K}_i$ is the discrete counterpart of the differential operator $\nabla \times (\rho(x) \nabla \times)$. The subscript i indicates that the discretization depends on the ith mesh. $\delta t_1, \ldots, \delta t_n$ are the time step lengths. The vectors $\boldsymbol{h}_{i,1}, \boldsymbol{h}_{i,2}, \boldsymbol{h}_{i,n}$ contain the tangential magnetic field components at the edges of the OcTree mesh at times $t_0, t_1, \ldots, t_n$. $f_1, \ldots, f_n$ are the values of the current f(t) at times $t_1, \ldots, t_n$. Here the right hand side $\mathbf{b_i}$, depends on the model parameter vector **m** if the source is active during the time stepping, that is if any $f_1, \ldots, f_n$ is nonzero.

The model parameter vector **m** is defined on the global mesh and contains the log-resistivity of each cell of this mesh. To obtain the resistivity for the cells of the ith local mesh, we must map from the global mesh to the local mesh. Our solution to this homogenization problem is to take the volume weighted average of the resistivity.

Solving equation 5 involves solving n systems of linear equations with the system matrices $\boldsymbol{M}_i + \delta t_k \boldsymbol{K}_i(\boldsymbol{m})$(k = 1, ..., n). Since the forward problem is discretized on the small local mesh, the use of sparse direct solvers is possible. These methods are preferable to iterative solvers because the factorizations can be reused for time steps of the same length or multiple sources grouped on the same mesh.

In a standard AEM survey, the time derivative of the vertical magnetic induction $\partial Bz/\partial t$ is measured. By denoting $d_{i,j}^{obs}$ the observed value of $\partial Bz/\partial t$ at the ith transmitter location, and the jth time channel, the predicted data can be computed from u_i by finite differening in time and interpolation in space and time. For time channel j and source-receiver pair i, we have

$$d_{i,j}(\boldsymbol{m}) = \boldsymbol{q}_{i,j}^T \boldsymbol{u}_i = \boldsymbol{q}_{i,j}^T [\boldsymbol{A}_i(\boldsymbol{m})]^{-1} \boldsymbol{b}_i(\boldsymbol{m}) \quad (8)$$

where the vector $\boldsymbol{q}_{i,j}$ contains the interpolation weights and finite difference coefficients.

INVERSE PROBLEM

To match the predicted and the observed data, we solve a minimization problem and seek a model vector **m*** such that

$$\boldsymbol{m}^* = \text{argmin } \phi(\mathbf{m}) \, , \quad (9)$$

where $\phi(\mathbf{m}) = \phi_d + \alpha R(\mathbf{m})$, and the data misfit

$$\phi_d(\mathbf{m}) = \sum_{i=1}^{n_s} \sum_{j=1}^{n_t} \frac{(d_{i,j}(\mathbf{m}) - d_{i,j}^{obs})^2}{(d_{i,j}^{std})^2} \quad (10)$$

n_s denotes the number of sources, n_t the number of measured time channels, $d_{i,j}^{std}$ the standard deviation of the datum $d_{i,j}^{obs}$, α the regularization parameter and R(**m**) a smoothness regularization functional. To minimize the non-linear objection function $\phi(\boldsymbol{m})$ we use the non-linear least squares method and reduce the data misfit until we reach the target data misfit.

FIELD EXAMPLE

In October 2008, a VTEM survey was flown over the Mt. Milligan porphyry deposit for Geoscience BC. The Mt. Milligan deposit, owned by Thompson Creek Metals Company Inc., is a Cu-Au porphyry deposit located within the Quesnel Terrane in British Columbia (see Figure 1). According to the Terrane Metals Corp. 2009 43-101 report (Mills et al., 2009), Mt. Milligan is a tabular, near-surface, alkalic copper-gold porphyry deposit that measures some 2,500 metres (m) north-south, 1,500 m east-west and is 400 m thick. The Main Zone is spatially associated with the MBX monzonite stock and Rainbow Dyke (see Figure 2). The mineralization and associated alteration are primarily hosted in volcanic rocks. Mineralization consists of pyrite, chalcopyrite and magnetite with bornite localized along intrusive-volcanic contacts. Copper-gold mineralization is primarily associated with potassic alteration which decreases in intensity outwards from the monzonite stocks. Pyrite content increases significantly outward from the stocks where it occurs in association with propylitic alteration, which forms a halo around the potassic-altered rocks. The Mt. Milligan copper-gold porphyry deposits contain Proven and Probable reserves of (Mills et al., 2009) 482 million tonnes (Mt) averaging 0.20% Cu and 0.39 grams per tonne (g/t) Au totaling 2.1 billion pounds copper and 6.0 million ounces gold.

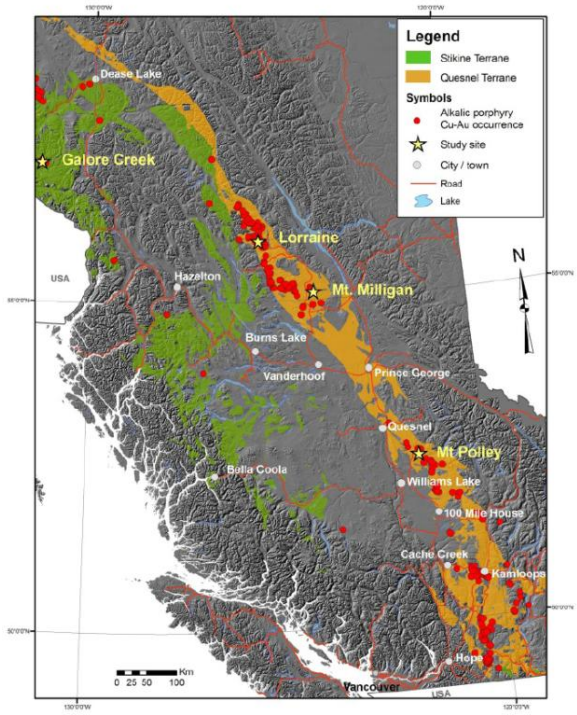

Figure 1 Mt. Milligan location in British Columbia Canada. The alkalic porphyry deposit lies in the Quesnel Terrane north of Prince George (after Devine, 2011).

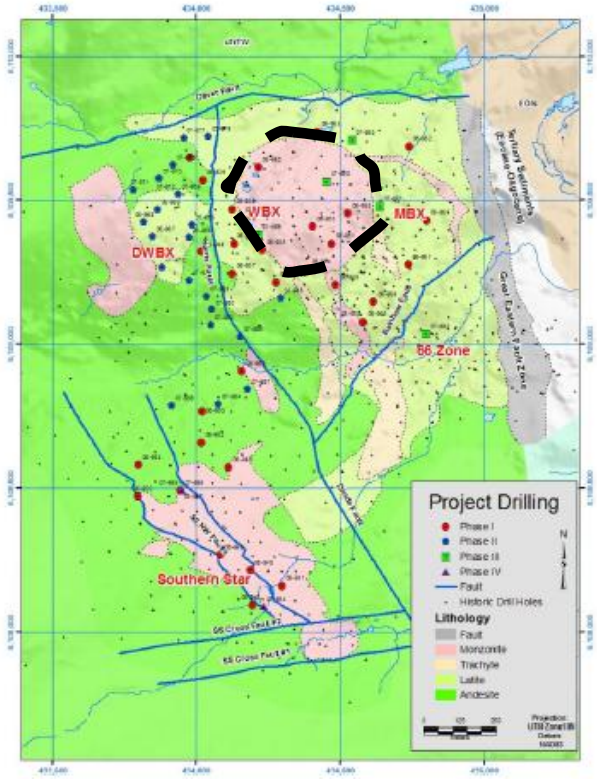

Figure 2 Mt. Milligan geology. The mineralization is hosted in 5 main zones (DWBX, Southern Star, 66, WBX and MBX). To the east of the deposit lies the Great Eastern Fault Zone and conductive tertiary sediments. The outline of the main monzonite MBX stalk is outlined in black.

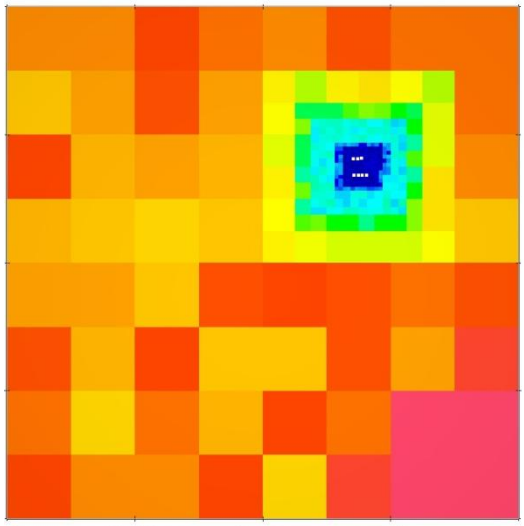

Figure 3 Planview portion of typical OcTree forward modelling mesh. A group of transmitters (white dots) are grouped together. The mesh is locally refined using fine cells (blue cells) around the transmitter and larger cells are used away from the transmitters (yellow and red cells).

The 2008 Mt. Milligan survey was part of the larger Quest survey and consisted of 13 VTEM lines for a total of 37.5 line-km of data. The airborne EM data were inverted using 144 different forward modelling meshes. The base inversion mesh contained cells each of which was 25 x 25 x 25 m in the x,y

and z directions (a single forward modelling mesh can be seen in Figure showing the localized refinement around the selected transmitters). The initial and reference models were set to be 200 ohm-m. The inversion ran to completion in around 13 hours running on 2 Intel Xeon x5600 series processors. The inversion result (Fig. 4) clearly images the Great Eastern Fault and the associated conductive sediments to the east of the Mt. Milligan deposit. The inversion also maps some higher conductivity zones associated with alteration. The inversion model shows the region around the monzonite MBX stalk to be of higher resistivity than the surrounding rocks which is consistent with physical rock properties obtained from the area (Mitchinson and Enkin, 2011)

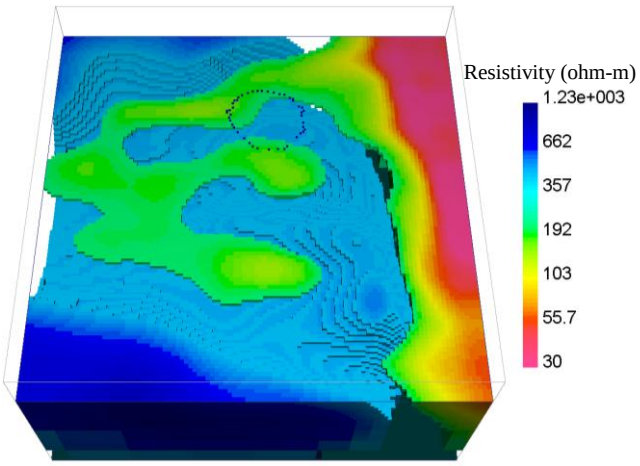

Figure 2 Mt. Milligan VTEM inversion at an elevation of 965m.

CONCLUSIONS

Airborne time-domain electromagnetic (EM) surveys are effective tools for mineral exploration, geologic mapping and environmental applications. The data are difficult to invert in 3D because of the number of sources and the size and scales of the computational domain. In this abstract we have proposed a new method to invert large-scale AEM datasets which partitions the forward problem into multiple meshes. Each mesh spans the full computational domain but uses fine mesh cells around the selected transmitters and receivers. This mesh refinement methodology results in a mesh having far fewer cells than the full inversion mesh. Since the forward modelling operation is the bottleneck for AEM inversions, this procedure results in a highly parallel algorithm that can handle arbitrarily large datasets and can deal with many scales in detail in the data. We applied our algorithm to VTEM field data from the Mt. Milligan porphyry deposits in British Columbia. The inversion results agree with the known geology and physical property measurements.

REFERENCES

Cox, L. H., and Zhdanov, M. S., 2008, Advanced computational methods of rapid and rigorous 3-D inversion of airborne electromagnetic data: Communications in Computational Physics, 3, 16–179.

Devine, F., 2011, Porphyry integration project: Bringing together geoscience and exploration datasets for British Columbias porphyry districts: Technical report, Geoscience BC.

Günther, T., Rücker, C., & Spitzer, K., 2006, Three dimensional modelling and inversion of dc resistivity data incorporating topography – II. Inversion: Geophysical Journal International, 166(2), 506–517.

Haber, E., & Heldmann, S., 2007, An OcTree multigrid method for quasi-static Maxwell's equations with highly discontinuous coefficients: Journal of Computational Physics, 65, 324–337.

Haber, E., Oldenburg, D., & Shektman, R., 2007, Inversion of time domain 3D electromagnetic data: Geophysical Journal International, 132, 1324–1335.

Horesh, L., & Haber, E., 2011, A second order discretization of Maxwell's equations in the quasi-static regime on OcTree grids: SIAM Journal on Scientific Computing, 33, 2805–2822.

Mills, K., J. Huang, G. Bosworth, S. Cowie, B. Borntraeger, H. Welhener, J. Collins, T. Bekhuys, and D. Labrenz, 2009, Technical Report - Feasibility Update Mt. Milligan Property - Northern BC: Technical report, Report to: Terrane Metals Corp. prepared by Wardrop.

Mitchinson, D. E., and R. J. Enkin, 2011, Continued investigations of physical property-geology relationships in porphyry-deposit settings in the Quest and Quest-West project area, Central British Columbia (NTS 093E, K, L, M, N): Technical report, Geoscience BC.

Schwarzbach, C., Börner, R.-U., & Spitzer, K., 2011, Three-dimensional adaptive higher order finite element simulation for geo-electromagnetics—a marine CSEM example: Geophysical Journal International, 187, 63–74.